12

Influence of Electric Fields and Boundary Conditions on the Flow Properties of Nematic-Filled Cells and Capillaries

Carlos I. Mendoza[1], Adalberto Corella-Madueño[2] and J. Adrián Reyes[3]
[1]*Institute of Materials Research, National Autonomous University of Mexico,*
[2]*Department of Physics, University of Sonora,*
[3]*Institute of Physics, National Autonomous University of Mexico,*
Mexico

1. Introduction

From a rheological point of view, nematic liquid crystals are interesting because they exhibit unique flow properties. Although some of these properties have been known for a long time, they continue to attract the attention and interest of the scientists. As a result, a large amount of theoretical, numerical, and experimental work has been produced in recent years. In particular, a number of publications treat the behavior of nematic liquid crystals in shear and Poiseuille flow fields (Denniston, Orlandini, and Yeomans 2001, Vicente Alonso, Wheeler, and Sluckin 2003, Marenduzzo, Orlandini, and Yeomans 2003, Marenduzzo, Orlandini, and Yeomans 2004, Guillen and Mendoza 2007, Medina and Mendoza 2008, Mendoza, Corella-Madueño, and Reyes 2008, Reyes, Corella-Madueño, and Mendoza 2008, Zakharov and Vakulenko, 2010).

On the other hand, it has been shown that the influence of an electric field strongly modifies the rheology of liquid crystals. This has considerable interest due to its possible application in microsystems since homogeneous fluids, like liquid crystals, present some advantages over conventional electrorheological fluids. This is mainly due to the fact that liquid crystals, in contrast to other active fluids, do not contain suspended particles, which is of particular importance for microsystems since small channels are easily obstructed by suspended particles. Also, they prevent agglomeration, sedimentation and abrasion problems (de Volder, Yoshida, Yokota, and Reynaerts 2006).

In this chapter we review recent theoretical results on the rheology of systems consisting of a flow-aligning nematic contained in cells and capillaries under a variety of different flow conditions and under the action of applied electric fields. In particular, we revise steady-state flows and the behavior of viscometric quantities like the local and apparent viscosities and the first normal stress differences. Among the important issues that were recently studied by us and by others is the possibility of multiple steady state solutions due to the competition between shear flow and electric field that give rise to a complex non-Newtonian response with regions of shear thickening and thinning. From these results one can construct a phase diagram in the electric field vs. shear flow space that displays regions for

which the system may have different steady-state configurations of the director's field. The selection of a given steady-state configuration depends on the history of the sample. Interestingly, as a consequence of the hysteresis of the system, this response may be asymmetric with respect to the direction of the shear flow. Possible applications of these phenomena are also discussed together with future research.

2. Fundamentals

Liquid crystal systems (De Gennes P.G. and Prost J. 1993) are well defined and specific phases of matter (mesophases) characterized by a noticeable anisotropy in many of their physical properties as solid crystals do, although they are able to flow. Liquid crystal phases that undergo a phase transition as a function of temperature (thermotropics), exist in relatively small intervals of temperature lying between solid crystals and isotropic liquids.

Liquid crystals are synthesized from organic molecules, some of which are elongated and uniaxial, so they can be represented as rigid rods; others are formed by disc-like molecules (Chandrasekhar S. 1992). This molecular anisotropy in shape is manifested macroscopically through the anisotropy of the mechanical, optical and transport properties of these substances.

Liquid crystals are classified by symmetry. As it is well known, isotropic liquids with spherically symmetric molecules are invariant under rotational, O(3), and translational, T(3), transformations. Thus, the group of symmetries of an isotropic liquid is O(3)×T(3). However, by decreasing the temperature of these liquids, the translational symmetry T(3) is usually broken corresponding to the isotropic liquid-solid transition. In contrast, for a liquid formed by anisotropic molecules, by diminishing the temperature the rotational symmetry is broken O(3) instead, which leads to the appearance of a liquid crystal. The mesophase for which only the rotational invariance has been broken is called nematic. The centers of mass of the molecules of a nematic have arbitrary positions whereas the principal axes of their molecules are spontaneously oriented along a preferred direction **n**, as shown in Fig. 1. If the temperature decreases even more, the symmetry T(3) is also partially broken. The mesophases exhibiting the translational symmetry T(2) are called smectics (see Fig. 1), and those having the symmetry T(1) are called columnar phases (not shown).

The elastic properties of liquid crystals determine their behavior in the presence of external fields and play an essential role in characterizing many of the electro-optical and magneto-optical effects occurring in them. In this work we shall adopt a phenomenological approach to describe these elastic and viscous properties. A liquid crystal will be considered as a continuum, so that its detailed molecular structure will be ignored. This approach is feasible because all the deformations observed experimentally have a minimum spatial extent that greatly exceed the dimensions of a nematic molecule. The macroscopic description of the Van der Waals forces between the liquid crystal molecules is given in terms of the following formula (Frank F. C. 1958) for the elastic contribution to the free-energy density:

$$F_{el} = \frac{1}{2}\int_V dV\left[K_{11}\left(\nabla\cdot\hat{n}\right)^2 + K_{22}(\hat{n}\cdot\nabla\times\hat{n})^2 + K_{33}(\hat{n}\cdot\nabla\times\hat{n})^2 \right]. \quad (1)$$

Here the unit vector **n** is the director, the elastic moduli K_{11}, K_{22}, and K_{33} describe, respectively, transverse bending (splay), torsion (twist), and longitudinal bending (bend)

deformations. The free energy of the LC cylinder has, in addition to the above elastic part, also an electromagnetic part due to the applied electrostatic field. As we have already discussed, the first contribution is given by Eq. (1). The electromagnetic free energy density, in MKS units,

$$F_{em} = \frac{1}{2}\int_v dV\left[\vec{\mathrm{E}}\cdot\vec{D}^* + \vec{B}\cdot\vec{H}^*\right] \tag{2}$$

where the displacement field D and the magnetic flux vector B are related to the electric field E and magnetic field H by means of the constitutive relations

$$\vec{D} = \varepsilon_0\varepsilon\cdot\vec{E}, \vec{B} = \mu_0\mu\cdot\vec{H}, \tag{4}$$

characterized specifically by dielectric and magnetic tensors (DeGennes P. G. and Prost. J. 1993)

$$\begin{aligned}\varepsilon_{ij} &= \varepsilon_\perp\delta_{ij} + \varepsilon_a n_i n_j \\ \mu_{ij} &= \delta_{ij}\end{aligned} \tag{5}$$

Here δ_{ij} is the Kronecker delta, $\varepsilon_a = \varepsilon_{\|} - \varepsilon_\perp$ is the dielectric anisotropy of the LC, $\varepsilon_\perp$ and $\varepsilon_{\|}$ represent the dielectric constants perpendicular and parallel to the director. Also, ε_0 and μ_0 are the dielectric permittivity and magnetic permeability constants in vacuum.

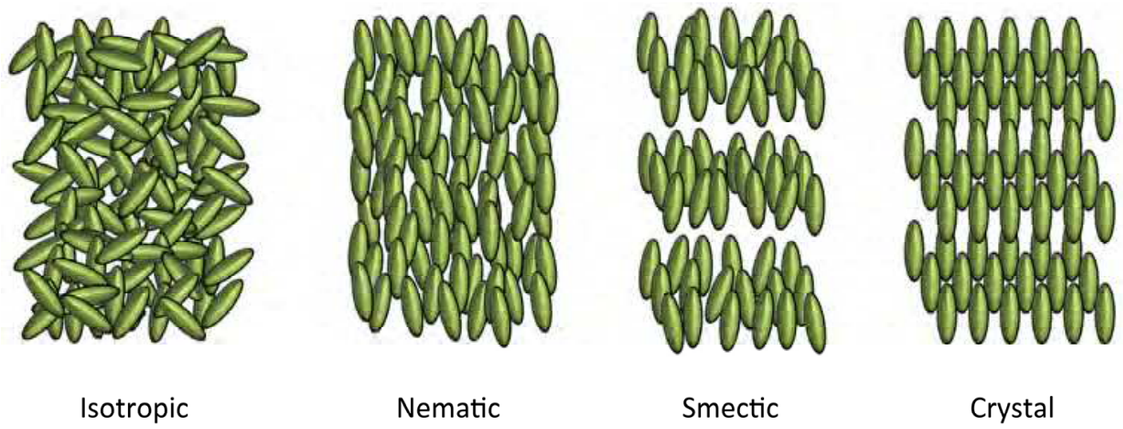

Fig. 1. Schematics of thermotropic liquid crystal phases in between the isotropic fluid and the crystal, arranged from left to right in order of increasing order and decreasing temperature.

3. Nematodynamics

The hydrodynamic description of complex condensed matter systems like superfluids, ferromagnets, polymeric solutions, etc. has been possible thanks to the deep understanding of the role played by the symmetries and thermodynamic properties of the system (Kadanoff and Martin P.C. 1963, Hohenberg and Matin P.C., Kalatnikov I. M. 1965). The extension of this linear hydrodynamic to liquid crystals has been started in the seventies, (Parodi O. 1970, Forster D. 1975), and in recent years it has been generalized to the nonlinear case and to more complex liquid crystal phases (Brand H. R. & Pleiner H. J. 1980).

The key idea of the hydrodynamic formalism is based on the observation that for most complex condensed matter systems in the limit of very large temporal and spatial scales, only a very small number of slow processes, compared with the enormous number of microscopic degrees of freedom, survives. The evolution of these processes is described by the evolution of the corresponding hydrodynamic variables that describe cooperative phenomena that are not to be relaxed in a finite time for a spatially homogeneous system. That is to say, the hydrodynamic variables are such that their Fourier transform satisfy the relation: $\omega(k\rightarrow 0)\rightarrow 0$. Moreover the hydrodynamic variables can be identified uniquely by utilizing conservation laws (global symmetries) and symmetry breaking assumptions, for spatio-temporal scales such that the microscopic degrees of freedom have already been relaxed. For these scales, the description of the systems is exact. When the microscopic degrees of freedom reach thermodynamic equilibrium (local equilibrium) one can use thermodynamics to follow the evolution of the slow variables. Thus, one has to consider a thermodynamic potential, for instance, the internal energy as a function of the system variables (Pleiner H. 1986, Pleiner H. 1988). In a second step we obtain the dynamics of the system by expressing the currents or thermodynamic fluxes in terms of their corresponding thermodynamic forces, which are the gradients of the conjugated thermodynamic variables, and performing a series expansion of the fluxes in powers of the forces. This expansion will be expressed in terms of dynamical phenomenological coefficients (transport coefficients) which can be determined only from an experiment or a microscopic theory. Then, we separate the fluxes in those for which the entropy is conserved (reversible part) and those that make the entropy to increase (irreversible part) and use classical thermodynamic laws to find the evolution equations for the hydrodynamic variables. After obtaining these equations for the liquid crystal, it is possible to include the effects of external fields like electromagnetic fields, stresses, thermal gradients, etc.

In what follows we sketch the steps of this theoretical formalism for nematics. The first class of hydrodynamic variables is associated with local conservation laws which express the fact that quantities like mass, momentum or energy cannot be locally destroyed or created and can only be transported. If $\rho(r,t)$, $g=\rho v(r,t)$ and $\varepsilon(r,t)$, where v is the hydrodynamic velocity, denote respectively, the density of these quantities, the corresponding conservation equations are ((Landau L.D. and Lifshitz E. 1964).

$$d\rho / dt + \rho \nabla_i v_i = 0 \tag{6}$$

$$dv_i / dt + \nabla_j \sigma_{ij} / \rho = 0 \tag{7}$$

$$d\left(e / \rho\right) / dt + \nabla_i j^e{}_i / \rho = 0 \,. \tag{8}$$

Here $d / dt = \partial / \partial t + v_i \nabla_i$ denotes the hydrodynamic velocity, σ_{ij} is the nematic's stress and j_i^e is the energy flow.

When a phase transition to the liquid crystal state occurs after reducing the temperature, the rotational symmetry O(3) is broken spontaneously and the number of hydrodynamic variables increase. Any rotation around an axis different from $\hat{n}$ transforms the system to a different and distinguishable state form that without rotation. This rotational symmetry broken is called spontaneous since the energy is a rotational invariant and there is no energy that favors one

orientation of $\hat{n}$ with respect to any other. This is equivalent to say that the state of the system becomes infinitely degenerate. Under these conditions, one soft variation of the degeneracy parameter is related to a slow relaxation of the system that increases as q→0. This type of behavior is the basic content of the Goldstone Theorem (Forster D. 1975). Therefore, the degeneracy parameter is related to the order parameter of the liquid crystal and adopts different structures for different mesophases. For a nematic phase the order parameter has the following form $Q_{ij} = S(n_i n_j - \delta_{ij} / 3)$, where S is the degree of order, i. e., S=0 for the isotropic phase and S=1 for a nematic phase having the molecules completely aligned. In agreement with this statement the dynamics of Q_{ij} is determined by that of **n**. In summary, the macroscopic state of a nematic can be described by means of two scalar variables that can be chosen as ρ(r,t), $e(\mathrm{r},t)$, one vectorial variable, g=ρv(r,t) and one tensorial variable Q_{ij} , that can be selected, for instance, as the anisotropic part of the dielectric tensor.

Since $\hat{n}$ is related to a conservation law, its balance equation is a dynamical equation of the form

$$\left[\partial / \partial t + v_j \nabla_j\right] n_i + Y_i = 0 \tag{9}$$

where Y_i is not a current, since its surface integral is not a flux, but a quasi-current. This quantity must be orthogonal to **n** to fulfill the nematic symmetry **n**→- **n**; however, there are other contributions to Y_i which does not come from the symmetries but from thermodynamic requirements.

If a specific physical situation is given, the state of the system can be described in terms of an appropriate thermodynamic potential. This can be chosen, for example, as the total free energy E, (Callen H. B. 1985)

$$E = eV = E(V, \rho V, gV, \rho V \nabla_j n_i, \rho V n_i, V\sigma) \tag{10}$$

where V denotes the volume of the system and σ is the entropy per unit of volume. From this assumption and using Euler's relation, we can derive the Gibbs' expression

$$de = \mu d\rho + T d\sigma + \vec{v} \cdot d\vec{g} + \Phi_{ij} d\nabla_j n_i + h_i dn_i, \tag{11}$$

and the Gibbs-Duhem's relation

$$p = -e + \mu\rho + T\sigma + \vec{v} \cdot \vec{g}\,. \tag{12}$$

Here μ is the chemical potential, Φ_{ij} y h_i are called the molecular fields, which are defined as the partial derivatives of the thermodynamic potential with respect to the corresponding conjugated variable. Since in equilibrium the state variables are constants, any inhomogeneous distribution of these variables takes the system out of equilibrium. For this reason the gradients of these quantities are taken as thermodynamic forces. Hence, the presence of ∇μ, ∇T, $\nabla_j n_i$ and $\nabla_j \Phi_{ij}$ give rise to irreversible processes in the system. The dynamical part of the hydrodynamic equations is obtained by expressing the currents σ_{ij}, j_i^e, and Y_i in terms of the thermodynamic variables T, μ, v_i, and Φ_{ij}. If additionally we separate in these expressions the reversible part, which does not generate entropy increase and it is

invariant under temporal inversion, from the irreversible part, which increases the entropy and is not invariant under the transformation t→-t, we obtain the following expressions for the fluxes (Landau L. D. and Lifshitz E. 1986, Plainer H. 1988)

$$\sigma_{ij} = \sigma_{ij}^{R} + \sigma_{ij}^{D} = p\delta_{ij} + \Phi_{kj}\nabla_i n_k - \lambda_{kji} h_k / 2 - \nu_{ijkm}\nabla_m v_k \tag{13}$$

$$Y_i = Y_i^{R} + Y_i^{D} = -\lambda_{kji}\nabla_j v_k / 2 + \delta_{ik}^{\perp} h_k / \gamma_1 \tag{14}$$

$$j_i^{e} = T j_i^{\sigma D} + v_j \sigma_{ij}^{D} \ . \tag{15}$$

In these equations the superscript indexes R and D denote, respectively, the reversible and irreversible or dissipative parts, and

$$\Phi_{il} = K_{ilmn}\nabla_n n_m \tag{16}$$

where

$$K_{ilmn} = K_1\delta_{il}^{\perp}\delta_{mn}^{\perp} + K_2 n_p n_q \varepsilon_{pli} + K_3 n_i n_m \delta_{lm}^{\perp} \ . \tag{17}$$

Here K_1, K_2 y K_3 are the elastic constants of the nematic and ε_{ijk} is the totally antisymmetric tensor of Levy-Civitta. The projector tensor is $\delta_{lm}^{\perp} = \delta_{ik} - n_i n_k$ and λ_{kji} can be expressed as

$$\lambda_{kji} = (\lambda - 1)\delta_{kj}^{\perp} n_i + (\lambda + 1)\delta_{ki}^{\perp} n_j . \tag{18}$$

In this expression $\lambda = \nu_1/\nu_2$, is the reversible parameter, also called flux alignment parameter, being ν_1 and ν_2 two of the five independent viscosities of the nematic. The molecular field h_k, that we have already defined as $h_k \equiv h_i' - \nabla_j \Phi_{ij}$, turns out to be explicitly

$$h_k = K_{kjnl}\nabla_j\nabla_l n_n + \delta_{kq}^{\perp}\left(\frac{1}{2}\partial / \partial n_q K_{pjkl} - \partial / \partial n_q K_{qjkl}\right)\nabla_l n_k \nabla_j n_p . \tag{19}$$

Finally, the viscous stress tensor ν_{ijkl} contains five independent viscosities for the nematic, ν_i, i=1,2,...,5

$$\begin{aligned} \nu_{ijkl} = {} & \nu_2(\delta_{jl}\delta_{ik} + \delta_{il}\delta_{jk}) + 2(\nu_1 + \nu_2 - 2\nu_3) n_i n_j n_k n_l + \\ & (\nu_3 - \nu_2)(n_j n_l \delta_{ik} + n_j n_k \delta_{il} + n_i n_k \delta_{jl} + n_i n_l \delta_{jk}) + (\nu_4 - \nu_2)\delta_{ij}\delta_{kl} \ . \\ & (\nu_5 + \nu_4 + \nu_2)(\delta_{ij} n_k n_l + \delta_{kl} n_i n_j) \end{aligned} \tag{20}$$

It should be mentioned that a different choice for this tensor has been done in the ELP formulation (Ericksen, J. L. 1960, Leslie, F. M. 1966, Parodi, 0. 1970). The complete stress tensor for this formulation is given by Eq.(39) which for this case replaces Eq.(13).

The second law of thermodynamics establishes that any irreversible process that occurs in the system should increase the entropy. Thus, the entropy obeys the following balance equation

$$\partial\sigma / \partial t + \nabla_i\left(\sigma v_i + j_i^{\sigma R} + j_i^{\sigma D}\right) = R / T \tag{21}$$

where R is the dissipation function for irreversible processes. This quantity can be interpreted as the energy per unit of volume dissipated by the microscopic degrees of freedom and divided by the temperature (R/T), represents the entropy production of the nematic. If, as we did previously, we relate Eq.(21) with Eqs. (6), (7), (8) and (9), by using the Gibbs' expression (11) and the expressions (13)-(21), we obtain an explicit formula for R, that is

$$\begin{aligned} R &= -\nabla_i (j_i^D - T o_{ij}^D \nabla_j v_i + h_i \delta_{ij}^{\perp} Y_j^D) - j_i^{\sigma D} \nabla_i T - \sigma_{ij}^D \nabla_j v_i + h_i \delta_{ij}^{\perp} Y_j^D \\ &= \frac{1}{2\gamma_1} h_i \delta_{ij}^{\perp} h_j + \frac{1}{2} \nu_{ijkl} \nabla_j v_i \nabla_l v_k + \frac{1}{2} \kappa_{ij} \nabla_i T \nabla_j T, \end{aligned} \tag{22}$$

where γ_1^{-1} is the rotational viscosity and the tensor κ_{ij} describes the heat conduction (thermal conductivity). The second law of thermodynamics requires R to be a definite positive form, which in turns implies that every single coefficient of the previous expression is positive. Notice that Eq.(22) implies as well that the dissipative currents and quasi-currents are given by the partial derivatives of the dissipation function, that is

$$j_i^{\sigma D} = \partial R / (\partial \nabla_i T) = \kappa_{ij} \nabla_j T, \tag{23}$$

$$\sigma_{ij}^D = \partial R / \partial (\nabla_j v_i) = \nu_{ijkl} \nabla_l v_k, \tag{24}$$

$$Y_k^D = \partial R / \partial h_k = \delta_{ik}^{\perp} h_i / \gamma_1 . \tag{25}$$

In summary equations (6), (7), (8), (9) and (22) constitute a complete set to describe the irreversible dynamics of a low molecular weight nematic (thermotropic) in absence of external fields.

4. Constitutive equations

It is usual that applied external fields like electric and magnetic fields, gravity, temperature gradients, pressure and concentration, shear and vortex flows carry out the nematic to a new equilibrium state so that these fields must be included in the hydrodynamic equations.

It is well known that for any polarizable medium an electric field E induces a polarization P =D-ε_0E, where D is the displacement electric vector. Now, in a nematic the molecular dipolar moments are oriented approximately parallel with respect to the long axis of the molecules. Thus, the induced polarization gives rise to a director orientation. In contrast the influence of the magnetic field in a nematic is much weaker and in general, the induced magnetization can be neglected. A very well known result based on conventional thermodynamic arguments establishes that the work associated to an electric field E =-$\nabla\Phi$, is given by $dw_{el} = -(1/2)\vec{E} \cdot \vec{D}$, which should be added to the Gibbs' expression (11) and to the Gibbs-Duhem's relation (12). By modifying these expressions and using a procedure completely analogous to the one we followed in the last section, it is possible to show that in the presence of an electric field Eq. (7) transforms into

$$dv_i / dt + \nabla_j \sigma_{ij} / \rho = \rho_E E_i + P_j \nabla_j E_i \tag{26}$$

where the charge density is given by $\rho_E = \varepsilon_0 \mathrm{div}\, D$. To linear order in the thermodynamic forces, the expression for σ_{ij} has to include in addition the electric contributions, so that we replace Eq. (13) by the expression

$$\sigma_{ij} = \sigma_{ij}^R + \sigma_{ij}^D = \tilde{p}\delta_{ij} + \Phi_{lj}\nabla_i n_l - (1/2)\lambda_{kji}h_k - \nu_{ijkl}\nabla_l v_k \tag{27}$$

with $\tilde{p} = p - \varepsilon E^2/2$. Analogously, the currents (14), now are given by

$$Y_i = Y_i^R + Y_i^D = -(1/2)\lambda_{kji}\nabla_j v_k + (1/\gamma_1)\delta_{ik}^{\perp}h_k - \zeta_{ijk}^e \nabla_j E_k \tag{28}$$

$$j_i^e = \sigma_{ij}^E E_j + \kappa_{ij}^E \nabla_j T + \nabla_j\left(\zeta_{kjl}^E h_k\right), \tag{29}$$

where σ_{ij}^E is the electric conductivity, and in consequence the entropy current is

$$j_i^{\sigma} = -\kappa_{ij}\nabla_j T - \kappa_{ij}^E E_j \ . \tag{30}$$

Here the material tensors of second rank, κ_{ij}^E and σ_{ij}^E have uniaxial form and each one should be expressed in terms of two dissipative transport coefficient, that is,

$$\alpha_{ij} = \alpha_{\perp}\delta_{ij}^{\perp} + \alpha_{\parallel} n_i n_j \ . \tag{31}$$

On the other hand, the third order tensor ζ_{kji}^E is irreversible and contains a dynamical coefficient, the flexoelectric coefficient ζ^E,

$$\zeta_{ijk}^E = \zeta^E(\delta_{ij}^{\perp}n_k + \delta_{ik}^{\perp}n_j). \tag{32}$$

Following the same steps we used to obtain Eq.(22), the dissipation function R show in this case additional terms which involve the electric field,

$$\begin{aligned} 2R = {} & h_i\delta_{ij}^{\perp}h_j + \nu_{ijkl}\nabla_j v_i \nabla_l v_k + \kappa_{ij}\nabla_i T\nabla_j T \\ & + \sigma_{ij}^E E_i E_j + \kappa_{ij}^E E_i \nabla_j T - \zeta_{ijk}^E h_i \nabla_j E_k . \end{aligned} \tag{33}$$

Most of the parameters involved in the hydrodynamic and electrodynamic equations for a nematic have been measured for different substances that show a uniaxial nematic phase. Among these one can mention the elastic constants (Blinov L. M. and Chigrinov V. G. 1994); specific heat, the flux alignment parameter λ and the viscosities ν_i, i=1,2...5, the inverse of the diffusion constant γ_1, the thermal conductivity (Ahlers, Cannell, Berge and Sakurai 1994), and the electric conductivity σ_{ij}^E.

Finally the dynamical equations for a nematic in an isothermal process can be obtained by inserting Eqs. (27) and (28) in Eqs. (7) and (9). This leads to

$$dv_i/dt + (1/\rho)\nabla_j\left[p\delta_{ij} + \Phi_{lj}\nabla_l n_i - \lambda_{kji}h_k - \nu_{ijkl}\nabla_l v_k\right] = 0 \tag{34}$$

$$dn_i/dt + (1/\gamma)\delta_{ik}^{\perp}h_k - \lambda_{kji}\nabla_j v_k = 0 \tag{35}$$

5. Apparent viscosity

The viscosity function or apparent viscosity connects the force per unit area and the magnitude of the local shear (Carlsson T. 1984). It depends on the orientation of the director through the expression

$$\eta(\theta) = (2\alpha_1 \sin^2\theta\cos^2\theta + (\alpha_5 - \alpha_2)\sin^2\theta + (\alpha_6 + \alpha_3)\cos^2\theta + \alpha_4)/2, \tag{36}$$

where α_1, α_2,α_3,α_5 and α_6 are the Leslie coefficients (Parodi O. 1970). Since the orientation angle θ is given by Eq. (35), from the above equation it follows that the dependence of η on θ indicates that the system is non-Newtonian in its behavior, in the sense that η is strongly dependent on the driving force. If we integrate the result over the cross section area of the flow we obtain the averaged apparent viscosity

$$\bar{\eta} = (1/A_t)\int_{A_t} \eta(\theta) dA \tag{37}$$

where A_t is the total area of the cross section.

6. First normal stress difference

One of the distinctive phenomena observed in the flow of liquid crystal polymers in the nematic state is that of a negative steady-state first normal stress difference, N_1, in shear flow over a range of shear rates. N_1 is zero or positive for isotropic fluids at rest over all shear rates, which means that the force developed due to the normal stresses, tends to push apart the two surfaces between which the material is sheared. In liquid crystalline solutions, positive normal stress differences are found at low and high shear rates, with negative values occurring at intermediate shear rates (Kiss G. and Porter R. S. 1978).

On the other hand, Marrucci et al (Marrucci G. and Maffettone 1989) have solved a two dimensional version of the Doi model for nematics (Doi M. and Edwards S.. F. 1986), in which the molecules are assumed to lie in the plane perpendicular to the vorticity axis, that is, in the plane parallel to both, the direction of the velocity and the direction of the velocity gradient. Despite this simplification, the predicted range of shear rates over which N_1 is negative, is in excellent agreement with observations. This result opens up the possibility that negative first normal stress differences may be predicted in a two dimensional flow.

We shall now examine the effects produced by the stresses generated during the reorientation process by calculating the viscometric functions that relate the shear and normal stress differences. For a planar geometry and using the convention in (Bird R. et al 1971) the first normal stress difference is defined by

$$N_1 = \sigma_{xx} - \sigma_{zz}, \tag{38}$$

where σ_{ij} are the components of the stress tensor of the nematic used by De Gennes (DeGennes J. P. and Prost J. 1993).

$$\begin{aligned}\sigma_{ij} = {} & \alpha_1 n_i n_j n_\mu n_\rho A_{\mu\rho} + \alpha_2 n_i \Omega_j + \alpha_3 n_j \Omega_i + \\ & \alpha_4 A_{ij} + \alpha_5 n_i n_\mu A_{\mu j} + \alpha_6 n_i n_\mu A_{\mu j}.\end{aligned} \tag{39}$$

Here $A_{ij}\equiv(1/2)(\partial v_i/\partial x_j+\partial v_i/\partial x_j)$ is the symmetric part of the velocity gradient and $\Omega\equiv dn/dt-(1/2)\nabla\times v\times n$ represents the rate of change of the director with respect to the background fluid. The α_i for i=1,..6, denote the Leslie coefficients of the nematic.

The integration of the first normal stress difference, Eq.(38) over the whole cell and along the velocity gradient direction renders the net force between the plates as a function of the Reynolds number, which is proportional to N

$$f = (1/A_t)\int_{A_t} N_1(\theta)dA \tag{40}$$

A positive force exerted by the fluid motion tends to push the plates apart, or otherwise, if the force is negative, the fluid tends to pull the plates close together.

7. Nematic cells under shear flow

In this section we study the flow properties of nematic-filled cells under shear flow. The cell geometry is important because many micro-fluidic devices are designed with channel-like shapes and its mathematical treatment is simpler as compared to the case of capillaries.

Liquid crystals and their electrorheological properties under flows with a constant shear rate over the height of the channel have been treated in a number of papers. However, in all of these papers the studies have focused on situations in which the anchoring was the same at all boundaries. Only recently, a systematic study of the influence of different boundary conditions on the shear flow was treated together with the influence of an applied electric field.

7.1 Hybrid-aligned nematic cell

First we are going to present the case of a hybrid-aligned nematic (HAN) cell since it is a common geometry used in devices (Guillen and Mendoza 2007). In this geometry, the director is aligned perpendicularly (also called homeotropic alignment) to one of the boundaries of the confining cell while it is parallel (also called homogeneous alignment) to the opposite boundary as shown in Fig. 2.

The separation between the plates l is small compared to the transverse dimensions L of the cell, which is under the action of a perpendicular electric field E. The director's configuration is given by

$$\hat{\mathbf{n}} = [\sin\theta(z), 0, \cos\theta(z)], \tag{41}$$

where $\theta(z)$ is the angle with respect to the z axis. We assume strong anchoring conditions at the plates of the cell

$$\theta(z=-l/2)=0, \quad \theta(z=l/2)=\pi/2. \tag{42}$$

As shear flow is applied as depicted in Fig. 2

$$\mathbf{v} = [v_x(z), 0, 0], \tag{43}$$

which satisfies the nonslip boundary conditions

$$v_x(z = \pm l/2) = \pm v_0. \tag{44}$$

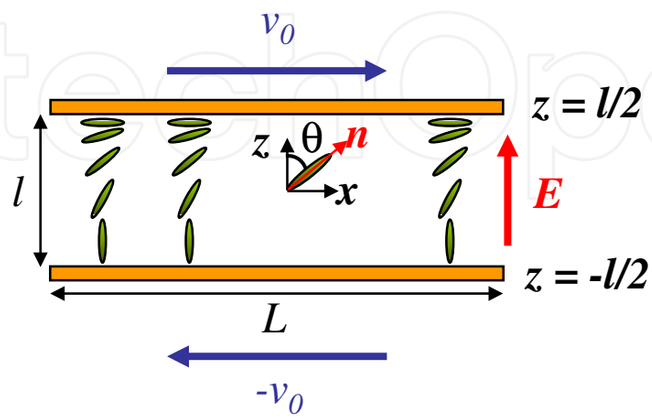

Fig. 2. Schematics of a HAN cell subjected to a normal electric field and a shear stress. Adapted from Guillen and Mendoza 2007.

Within the framework of the Ericksen, Leslie, and Parodi theory one can obtain the torque acting on a sheared molecule,

$$T_v = (\alpha_3 \sin^2\theta - \alpha_2 \cos^2\theta)\frac{dv_x}{dz}. \tag{45}$$

A second torque that acts on the LC molecules is due to the electric field

$$T_{el} = -\frac{\varepsilon_a \varepsilon_0}{2} E^2 \sin(2\theta), \tag{46}$$

An elastic torque can be derived form the Frank-Oseen elastic energy to give

$$T_e = (K_1 \sin^2\theta + K_3 \cos^2\theta)\left(\frac{d^2\theta}{dz^2}\right) + (K_1 - K_3)\sin\theta\cos\theta\left(\frac{d\theta}{dz}\right)^2. \tag{47}$$

Finally, the rotational inertia and viscous damping gives the following contribution to the torques

$$T_{dyn} = I\frac{d^2\theta}{dt^2} + \gamma\frac{d\theta}{dt}, \tag{48}$$

All the above contributions result in the differential equation for the director´s orientation that describes the equilibrium of torques

$$I\frac{d^2\theta}{dt^2}+\gamma\frac{d\theta}{dt}=(K_1\sin^2\theta+K_3\cos^2\theta)\left(\frac{d^2\theta}{dz^2}\right)+(K_1-K_3)\sin\theta\cos\theta\left(\frac{d\theta}{dz}\right)^2-\frac{\varepsilon_a\varepsilon_0}{2}E^2\sin(2\theta)+(\alpha_3\sin^2\theta-\alpha_2\cos^2\theta)\frac{dv_x}{dz}. \quad (49)$$

Since we are only interested in the final stationary state, the above equation reduces to (Guillen and Mendoza 2007)

$$\frac{d^2\theta}{d\varsigma^2}-q\sin(2\theta)+\frac{m}{\eta(\theta)}(\alpha_3\sin^2\theta-\alpha_2\cos^2\theta)=0, \quad (50)$$

where we have used the linear momentum conservation equation

$$\frac{d}{dz}\left[\eta(\theta)\frac{dv_x}{dz}\right]=0, \quad (51)$$

with η(θ) the position dependent viscosity of the liquid crystal given by Eq. (36), and we have assumed the equal elastic constant approximation. Also, we have defined a dimensionless field strength

$$q\equiv\frac{\varepsilon_a\varepsilon_0}{2K}l^2E^2 \quad (52)$$

a dimensionless shear rate

$$m\equiv\frac{lv_0c(q,m)}{K} \quad (53)$$

$$c(q,m)=\frac{2}{\int_{-1/2}^{1/2}d\varsigma'/\eta[\theta(\varsigma')]}$$

and the normalized variable $\zeta\equiv z/l$.

Equation (50) can be solved numerically using the "shooting" method to obtain the stationary configuration of the nematic's director.

Explicit numerical results are given for the particular case of the flow-aligning liquid crystal 4′-*n*-pentyl-4-cyanobiphenyl (5CB) with the following parameters T = 10 °C with T_{IN} = 35 °C, κ = 1.316, K_1 = 1.2_10^{-11} N, α_1 = −0.0060 Pa s, α_2 = −0.0812 Pa s, α_3 = −0.0036 Pa s, α_4 = 0.0652 Pa s, α_5 = 0.0640 Pa s, α_6 = −0.0208 Pa s, γ_1 = 0.0777 Pa s, γ_2 = −0.0848 Pa s.

In Fig. 3 we show the orientational profile for various values of q and m. We observe a tendency of the molecules to align with the direction of the electric field. In contrast, θ

increases as the value of m increases, for m>0, which means that the molecules tend to be aligned with the direction of the flow. On the other hand, for m<0, a remarkable difference is observed. In this case the cell shows two different regions, in the lower part of the cell, where the effect of the flow dominates, the molecules are tilted to the left whilst on the upper part, where the anchoring dominates, they are tilted to the right.

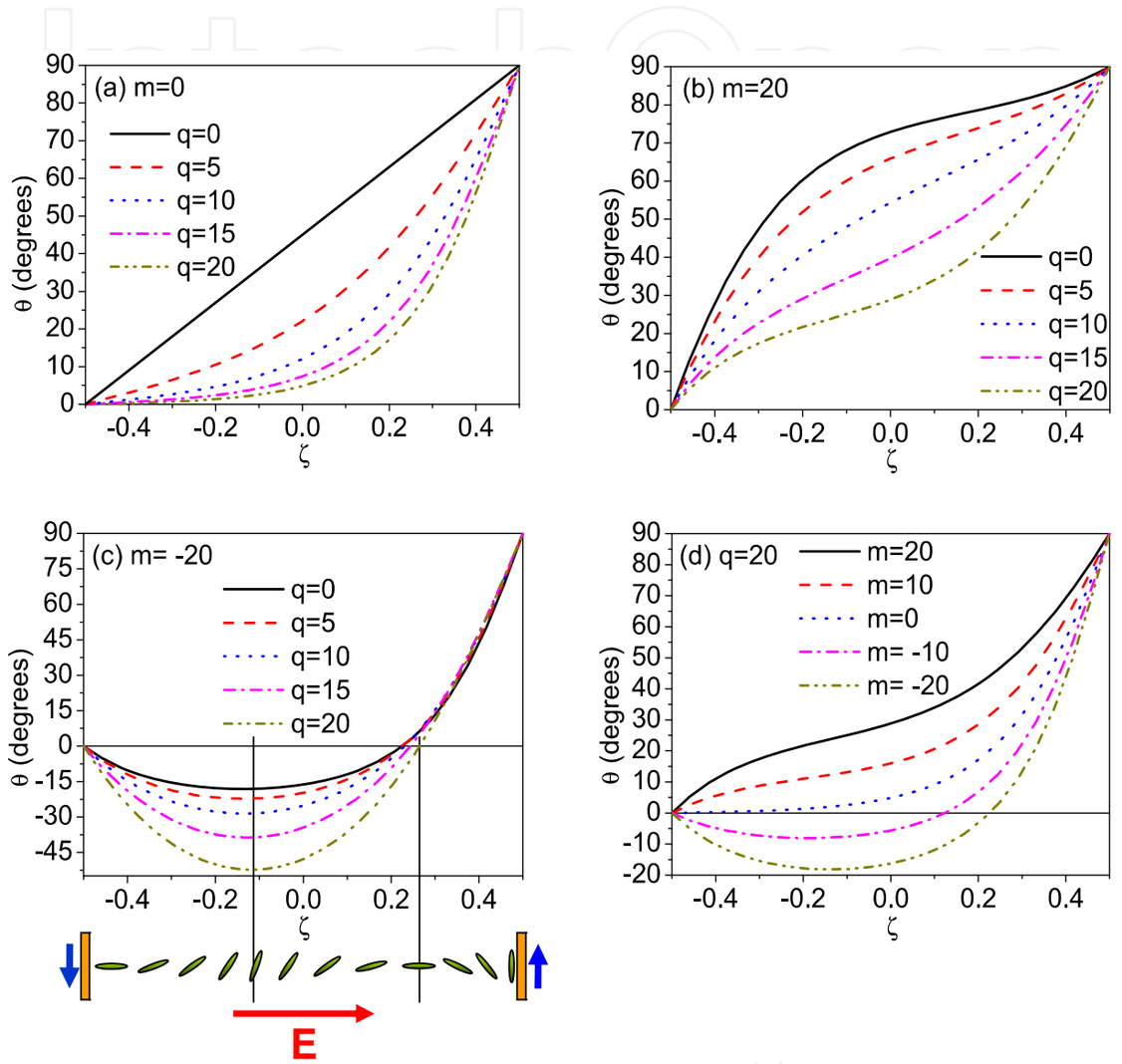

Fig. 3. Nematic's orientation θ as function of its position in the cell, ζ. Adapted from Guillen and Mendoza 2007.

The velocity profiles can be obtained from Eq. (51) and are shown in Fig. 4. Note the different behavior between a positive and a negative flow.

The position dependent viscosity can be calculated from Eq. (36) and it is shown in Fig. 5. It is maximum at the lower plate where the molecules are perpendicular to the direction of flow and minimum at the upper plate where the molecules are parallel to the direction of the flow. At intermediate positions the viscosity takes intermediate values.

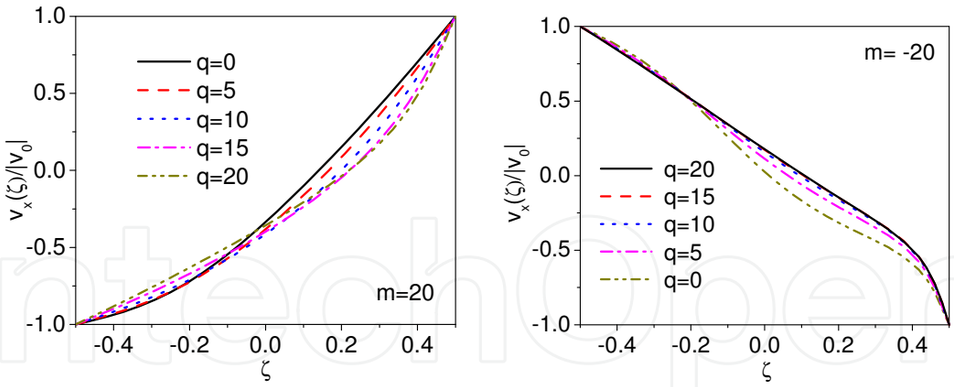

Fig. 4. Velocity profiles. Adapted from Guillen and Mendoza 2007.

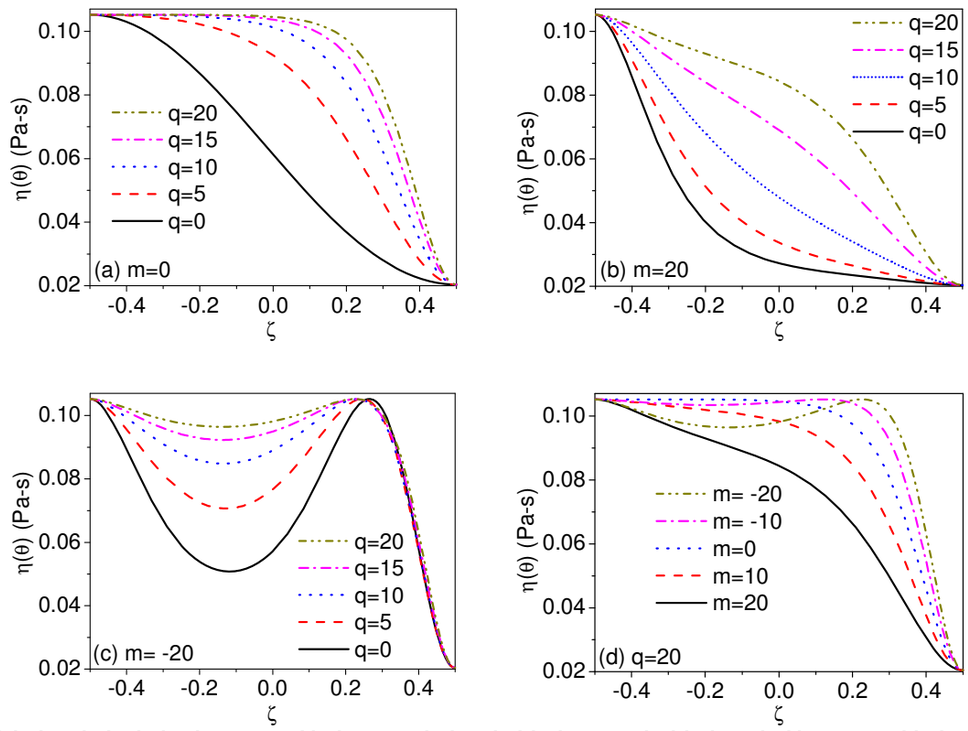

Fig. 5. Local viscosity for different values of the electric field and the shear flow. Adapted from Guillen and Mendoza 2007.

The averaged apparent viscosity [Eq. (37)] is depicted in Fig. 6. We observe a moderate electrorheological effect and an interesting non-Newtonian behavior with alternate regions of shear thickening (shaded region) and thinning.

Finally, the first normal stress difference

$$N_1[\theta(\varsigma)] = -\frac{|v_0|}{2l}\sin 2\theta(\alpha_1 \cos 2\theta + \alpha_2 + \alpha_3)\frac{d\bar{v}_x}{d\varsigma} + \frac{K}{l^2}\left(\frac{d\theta}{d\varsigma}\right)^2. \tag{54}$$

is plotted in Fig. 7 and the corresponding averaged value is shown in Fig. 8

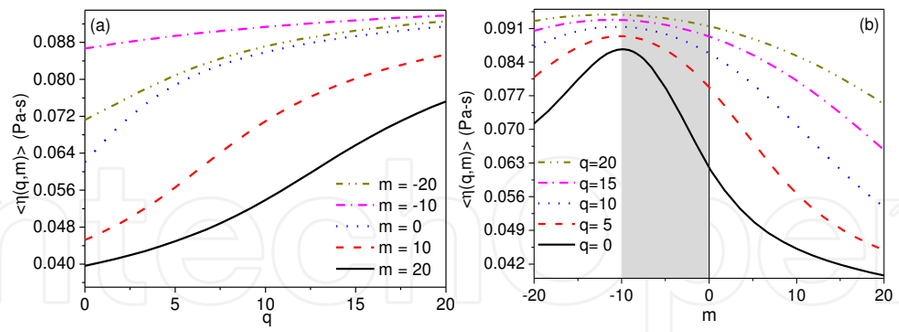

Fig. 6. Averaged apparent viscosity. Adapted from Guillen and Mendoza 2007.

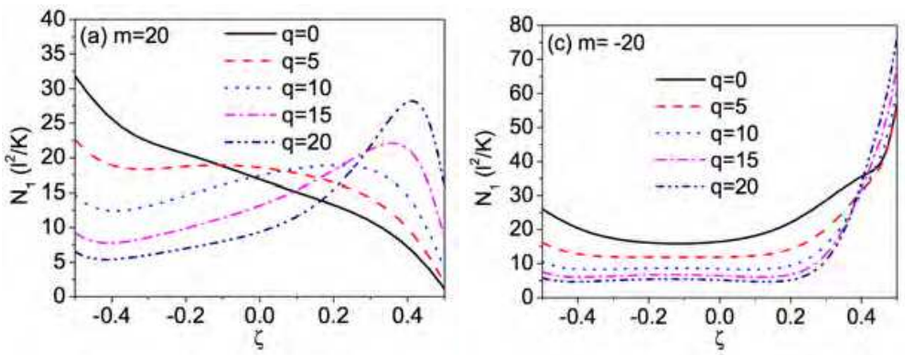

Fig. 7. First normal stress difference. Adapted from Guillen and Mendoza 2007.

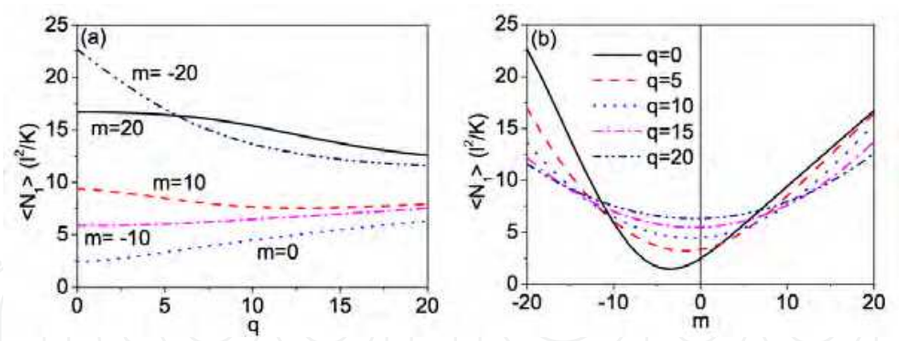

Fig. 8. Averaged first normal stress difference. Adapted from Guillen and Mendoza 2007.

7.2 Homogeneous nematic cell

In this subsection we study the flow of a homogeneous nematic cell as depicted in Fig. 9.

The only difference of this cell as compared to the HAN cell is that here the alignment is homogeneous at both plates. At first sight one may think that this small difference may only produce slight changes in the rheological behavior of the cell. However, this is not the case and a completely different behavior arises. The most striking feature is the appearance of multiple steady-state configurations for certain combinations of the applied electric field and shear flow (Medina and Mendoza 2008).

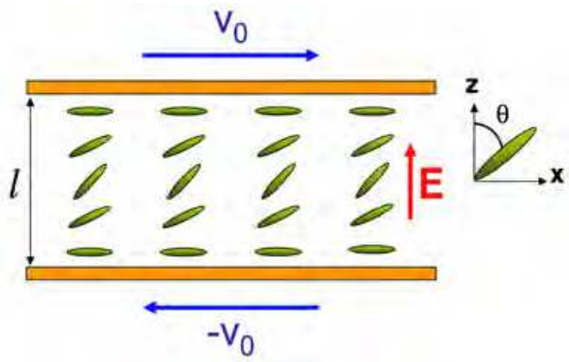

Fig. 9. Schematics of a homogeneous cell subjected to a normal electric field and a shear stress. Adapted from Medina and Mendoza 2008.

Using again the theory of Ericksen, Leslie, and Parodi together with the momentum conservation we obtain the differential equations that govern the steady state of the system

$$0 = \left(\sin^2\theta + \kappa\cos^2\theta\right)\frac{\mathrm{d}^2\theta}{\mathrm{d}\varsigma^2} + (1-\kappa)\sin\theta\cos\theta\left(\frac{\mathrm{d}\theta}{\mathrm{d}\varsigma}\right)^2 - q\sin(2\theta) + \frac{m}{\eta(\theta)}\left(\alpha_3\sin^2\theta - \alpha_2\cos^2\theta\right), \tag{55}$$

Here α_i are the Leslie viscosities and $\kappa \equiv K_3/K_1$, with the homogeneous

$$\theta(\varsigma = \pm 1/2) = \pi/2, \tag{56}$$

and non-slip boundary conditions.

The stationary configuration of the nematic's director can be found by solving Eq. (55) numerically using the "shooting" method. Results are presented for 5CB as before.

In Fig. 10 we show the nematic's configuration for different values of the applied electric field, q, without flow (a) and with flow (b). In this last case two sets of solutions of Eq. (55) are shown.

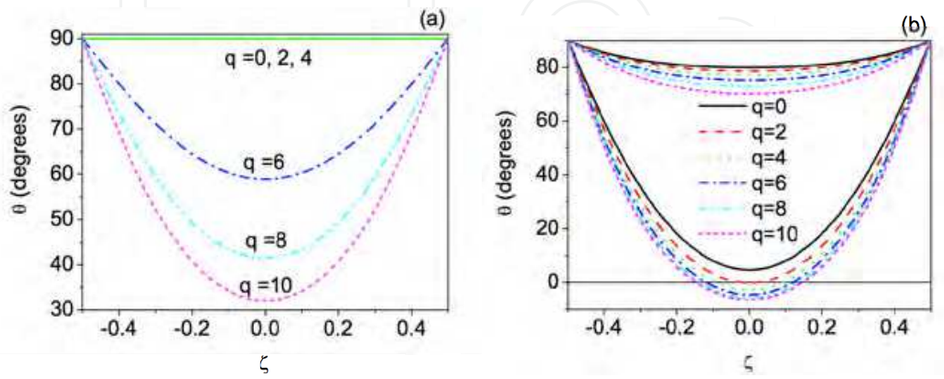

Fig. 10. Nematic's configuration for (a) m=0 and (b) m=20. In the latter case two solutions are shown, for the second set of solutions we plot 180^o - θ. Adapted from Medina and Mendoza 2008.

In Fig. 11 we show the nematic's configuration for q=2 and different values of the shear flow. The case m=5 lies in a region where exist only one solution of Eq. (55) while the case m=10 lies in the region where Eq. (55) accepts multiple solutions. A phase diagram in the q-|m| space is also shown in Fig. 11 that separates the region with only one solution from the region with multiple solutions. In the lower right panel we sketch the steady-state nematic's configuration for these cases. The selection of one of the configurations over the other depends on the history of the sample as exemplified in Fig. 12. In this figure, we have recasted the phase diagram drawing the positive and negative parts of the m-axis and considered two different processes depicted by the arrows in the phase diagram. The two processes start at zero applied electric field, but with opposite starting shear flows (points A and A′ in the diagram). Then, following the processes depicted by the arrows in the phase diagram they arrive to the same final q, m pair with different configurations (point B′).

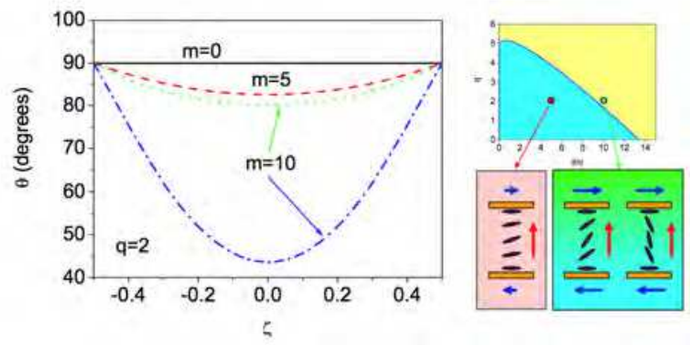

Fig. 11. Left: Nematic's configuration. Right up: Phase diagram showing the region (blue) with unique steady-state solutions and a region (yellow) with multiple solutions. Right down: Sketch of the configurations. Adapted from Medina and Mendoza 2008.

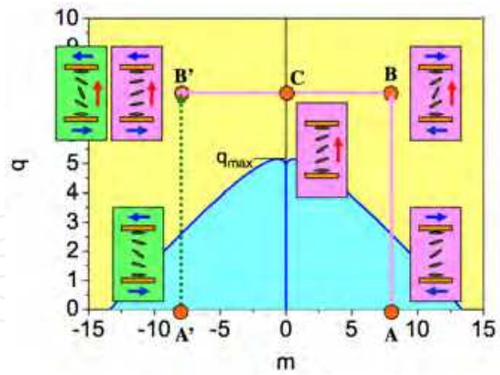

Fig. 12. Sketch of two possible trajectories in the phase diagram that gives rise to two different steady states for a given pair q and m (point B′). Adapted from Medina and Mendoza 2008.

In Fig. 13 we show the averaged viscosity as function of m for the trajectory starting at point A in Fig. 12. We observe an interesting non-Newtonian behavior with alternate regions of shear thickening and thinning. The second trajectory (the one starting at A′ in Fig. 12) would produce the same curves for the viscosity but interchanging m with –m. A moderate electrorheological effect is also evident in this figure.

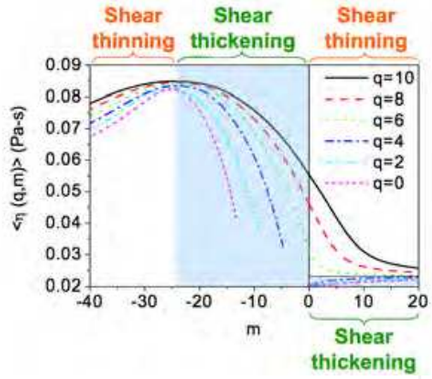

Fig. 13. Averaged apparent viscosity as a function of m showing regions of shear thickening and shear thinning. Adapted from Medina and Mendoza 2008.

In summary, we have shown that nematic cells are very sensitive to the boundary conditions at the plates of the cell. A HAN cell and a homogeneous cell behave in a completely different way, the homogeneous cell showing regions of multiple steady-state configurations that give rise to a history dependent rheological behavior that is absent in the HAN case. Both cases show complex non-Newtonian behavior with regions of shear thickening and thinning. Homeotropic cells and weak anchoring conditions remain to explore.

8. Nematic capillaries

In this section we study the flow properties of nematic-filled capillaries under the action of an electric field for two different flow conditions. In first place we treat the case of capillaries subjected to a pressure gradient and in second place we consider the case of a Couette flow.

8.1 Hybrid nematic capillary under Poiseuille flow

We consider a capillary consisting of two coaxial cylinders whose core is filled with a nematic liquid crystal subjected to the simultaneous action of both a pressure gradient applied parallel to the axis of the cylinders (Poiseuille flow) and a radial low frequency electric field as depicted in Fig. 14 (Mendoza, Corella-Madueño, and Reyes 2008).

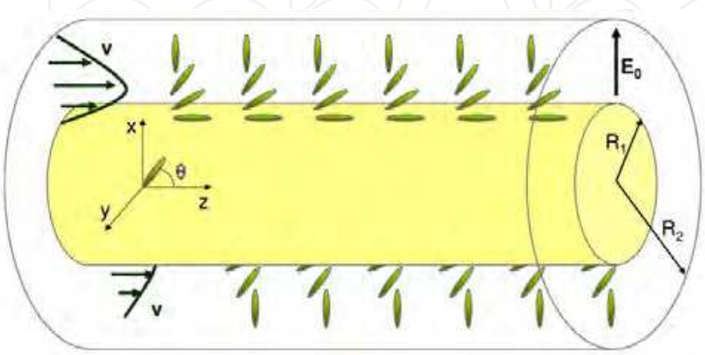

Fig. 14. Schematics of a nematic liquid crystal confined by two coaxial cylinders and subjected to a radial electric field and a pressure gradient. Adapted from Mendoza, Corella-Madueño, and Reyes 2008.

The nematic's director in cylindrical coordinates can be written as

$$\hat{\mathbf{n}} = [\sin\theta(r), 0, \cos\theta(r)], \tag{57}$$

with the hybrid hard anchoring conditions

$$\theta(r = R_1) = 0, \quad \theta(r = R_2) = \pi/2 \tag{58}$$

The constant pressure drop along the axis of the cylinders produces a flow profile given by

$$\mathbf{v} = [0, 0, v_z(r)], \tag{59}$$

with the non slip boundary conditions

$$v_z(r = R_1) = 0, \quad v_z(r = R_2) = 0. \tag{60}$$

The nematodynamic equations adopt a more involved look, as compared to the case of the cells. The reader can find the appropriate expressions in (Mendoza, Corella, Reyes 2008). Here we just present the relevant results using as in the previous sections a 5CB nematic liquid crystal.

In Fig. 15 we show the nematic's configuration as function of $x \equiv r/R_2$, parametrized with q, the ratio of the electric and elastic energies, and Λ, the ratio of the hydrodynamic and elastic energies (Mendoza, Corella-Madueño, Reyes 2008). The undistorted state corresponding to $\Lambda = 0$ and $q = 0$ is similar to the escaped configuration. For $q = 50$, $\hat{\mathbf{n}}$ is much more aligned with the radial direction than for $q = 0$. This is so because the director tends to be parallel to the electric field. For positive $\Lambda > 0$, corresponding to negative velocity, $\hat{\mathbf{n}}$ tends to be axially aligned, whereas for negative $\Lambda < 0$ the trend is the opposite. In contrast, for $q = 50$ the influence of the pressure gradient is influenced by the electric field for regions near the inner cylinder.

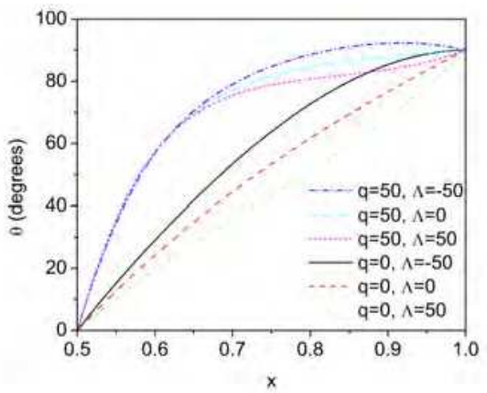

Fig. 15. Nematic's configuration θ as a function of the position $x \equiv r/R_2$ for 5CB and $R_1/R_2=0.5$. Adapted from Mendoza, Corella-Madueño, and Reyes 2008.

In Fig. 16 we show a typical velocity profile for a given value of the electric field and different values of Λ. This figure exhibits a clear difference in the magnitude of the velocity between forward and backward flows, which is a consequence of the asymmetry of the undistorted director's configuration (so called escaped configuration).

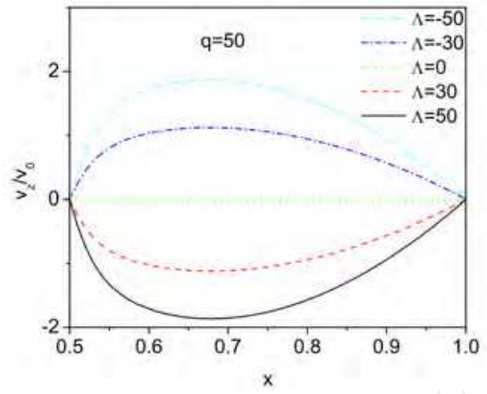

Fig. 16. Velocity profiles for a given q, and different values of Λ.

Moreover, the extreme of the curves, representing a vanishing shear stress, are closer to the inner cylinder for all the curves, with no significant dependence on the value of Λ. This behavior is different from a Newtonian fluid for which the maximum is approximately at the middle of the distance between both cylinders.

Fig. 17 presents the averaged apparent viscosity for this configuration. Note the non-Newtonian behavior of the system and the non-symmetric response with respect to the direction of the flow. In particular, in Fig. 17b we observe that for a given value of the electric field and for the range of flow considered the viscosity decreases as Λ increases. This means that for backward flow (Λ>0) the viscosity decreases as the magnitude of the flow increases whereas for forward flow (Λ<0) the viscosity increases as the magnitude of the flow increases. Therefore, we have flow thinning in one direction and flow thickening in the other. This directional response is due to the fact that the initial undistorted nematic configuration is asymmetrical. Even more, for the forward case most of the mechanical energy is elastically accumulated in distorting the nematic's configuration instead of being used to move the fluid, as compared to the backward case. In this sense the undistorted configuration is working like a biased spring inherent to the liquid, stiffer in one direction than in the other.

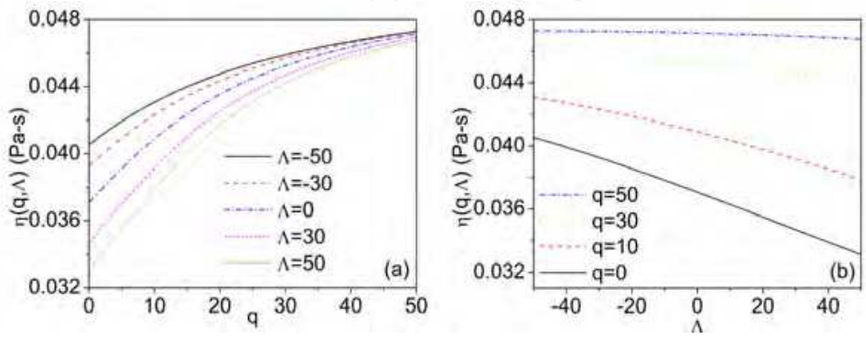

Fig. 17. Averaged apparent viscosity as a function of (a) the electric field q and (b) the pressure gradient Λ.

The averaged first normal stress difference is shown in Fig. 18. Panel (a) shows that N_1 depends almost linearly on q for backward flow, $\Lambda = -50$, whereas it has a minimum in q =

10 for forward flow $\Lambda = 50$. Panel (b) displays clearly the contrast between forward and backward flows for small values of q where a local minimum moves to the right as Λ increases. This shows that the directional dependence of this confined nematic can be electrically controlled.

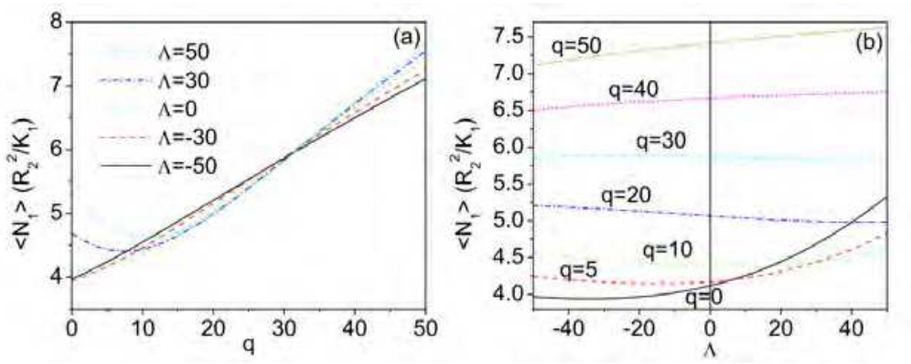

Fig. 18. Averaged first normal stress difference as function of (a) q and (b) Λ. Adapted from Mendoza, Corella-Madueño, and Reyes 2008. Adapted from Mendoza, Corella-Madueño, and Reyes 2008.

8.2 Homogeneous nematic capillary under a Couette flow

In this subsection we are going to present the case of a homogeneous nematic capillary subjected to a Couette flow and a radial electric field as shown in Fig. 19 (Reyes, Corella-Madueño, and Mendoza 2008). The inner cylinder is rotating with angular velocity Ω_1 and the outer cylinder with angular velocity Ω_2. This case resembles the one corresponding to the homogeneous cell, and in fact the phenomenology is very similar.

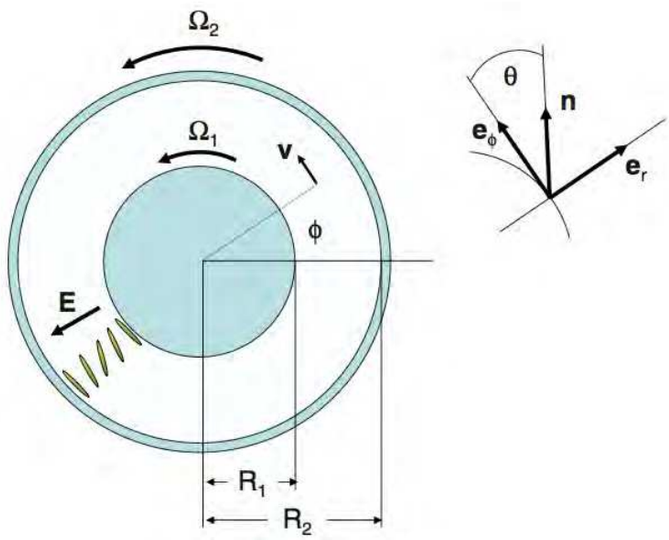

Fig. 19. Sketch of a nematic liquid crystal confined by two rotating coaxial cylinders and subjected to a radial electric field. Adapted from Reyes, Corella-Madueño, and Mendoza 2008.

According to the figure, the director can be written as

$$\hat{\mathbf{n}} = \sin\,\theta(r)\mathbf{e}_r + \cos\,\theta(r)\mathbf{e}_\phi, \tag{61}$$

and the velocity as

$$\mathbf{v} = \omega(r)r\mathbf{e}_\phi, \tag{62}$$

As in the previous situations, we are considering hard anchoring and non-slip boundary conditions at the cylinders

$$\theta(R_1) = 0, \quad \theta(R_2) = 0, \tag{63}$$

and

$$\omega(R_1) = \Omega_1, \quad \omega(R_2) = \Omega_2. \tag{64}$$

The orientational configuration for 5CB is shown in the left panel of Fig. 20. In (a) for q=20 and different values of ΔΩ. The angle grows from zero up to a maximum value, then, it decreases to zero at the outer cylinder. This maximum increases as we increase the value of ΔΩ. This simply means that the nematic's molecules tend to be more aligned with the flow

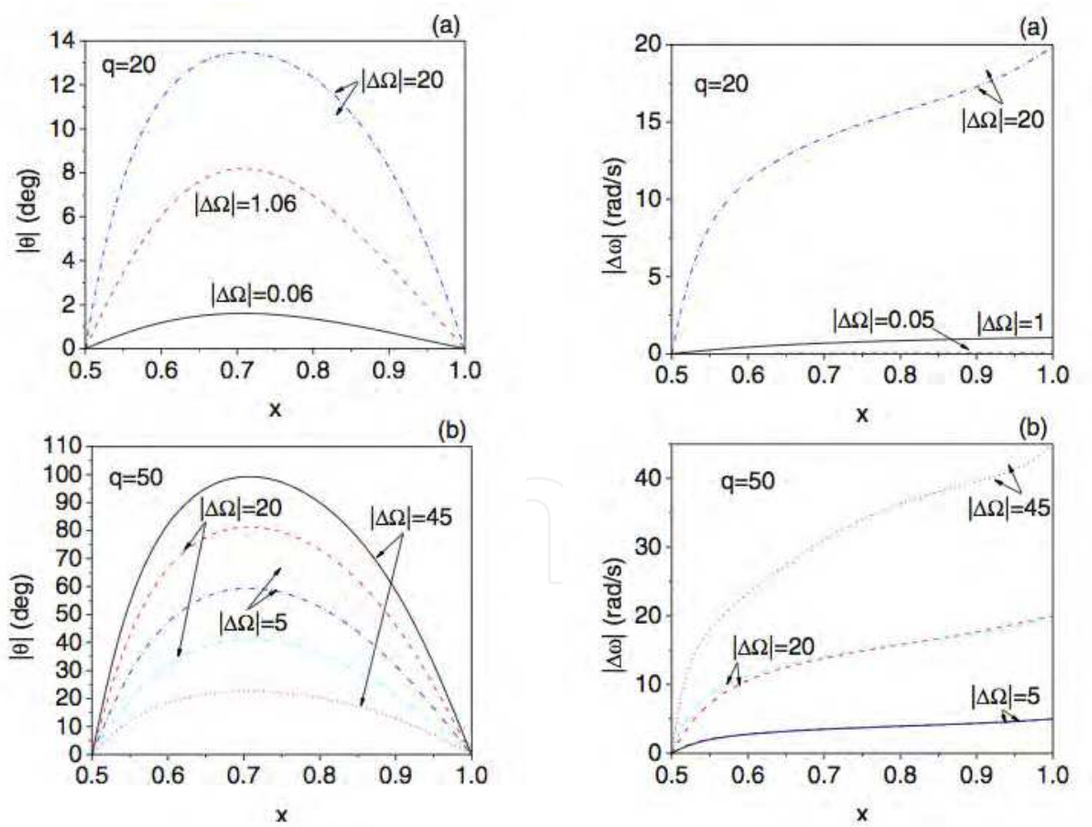

Fig. 20. Left panels: Nematic's configuration as a function of x for R_1/R_2=0.5 (a) q=20 and (b) q=50. Right panels: Velocity profiles as a function of x (a) q=20 and (b) q=50. The units of ΔΩ are rad/s. Adapted from Reyes, Corella-Madueño, and Mendoza 2008.

as it increases. As we can see, for the largest value of ΔΩ shown, there are two possible stationary configurations. In (b) we plot the same as in (a) but for q=50. In this case for any value of ΔΩ the system may adopt multiple steady-state solutions. Here, we have plotted two different possible solutions. In the right panels we plot the corresponding velocity profiles.

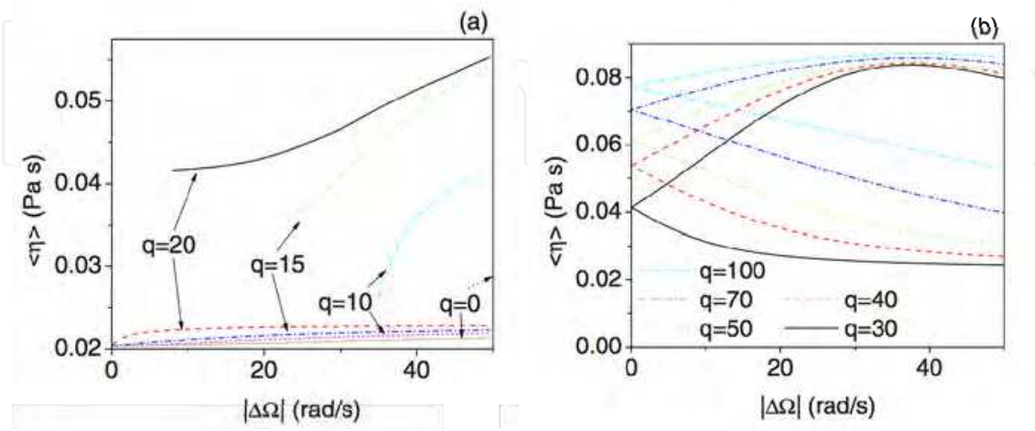

Fig. 21. Averaged apparent viscosity as a function of ΔΩ for (a) $q \leq 21$ and (b) $q \geq 21$. Adapted from Reyes, Corella-Madueño, and Mendoza 2008.

In Fig. 21 we present the average viscosity as a function of |ΔΩ|. Notice that the electrorheological effect is less pronounced for larger values of the shear flow since the cylinder's rotation turns the nematic perpendicularly to the electric field and as a consequence its influence is reduced.

9. Conclusion

We have presented a series of results that characterize the flow behavior of a flow-aligning thermotropic liquid crystal (5CB) under the action of an applied electric field in a variety of different flow geometries and boundary conditions. It is clear from these results that the influence of the boundary is enormous and may lead to completely different behaviors. Among the interesting results we can mention the existence of a rich non-Newtonian response with regions of shear thinning and thickening, a moderate electrorheological effect and a history dependent directional response.

10. Acknowledgment

CIM acknowledges partial financial support provided by DGAPA-UNAM through grant DGAPA IN-115010.

11. References

Ahlers G., Cannell D. S., Berge L. I. and Sakurai S, (1994) Thermal conductivity of the nematic liquid crystal 4-*n*-pentyl-4'-cyanobiphenyl, Phys. Rev. E Vol. 49, pp. 545

Arai, T. & Kragic, D. (1999). Variability of Wind and Wind Power, In: *Wind Power,* S.M. Muyeen, (Ed.), 289-321, Scyio, ISBN 978-953-7619-81-7, Vukovar, Croatia

Bird R. B., Armstrong R. C. and Hassager O., Dynamic of Polymeric Liquids, (Wiley, New York, 1977) Vol 1r D. (1989). Handbook of Differential Equation, Academic Press, New York Blinov L. M. and Chigrinov V. G., Electrooptic Effects in Liquid Crystal Materials (Springer, New York, 1994)

Brand H. R. and Pleiner, H., (1980). Nonlinear reversible hydrodynamics of liquid crystals and crystals, J. Phys (Paris) vol. 41, pp. 553

Brand H. R. and Pleiner H., (1982). Number of elastic coefficients in a biaxial nematic liquid crystal, Phys. Rev. A vol. 26, pp. 1783

Callen H. B., Thermodynamics and an Introduction to Thermostatistics (Wiley,New York, 1985) 2a. edición

Carlsson T., (1984). Theoretical Investigation of the Shear Flow of Nematic Liquid Crystals with the Leslie Viscosity $a_3 > 0$: Hydrodynamic Analogue of First Order Phase Transitions, Mol. Cryst. Vol. 104, pp. 307-334.

Chandrasekhar S., Liquid Crystals (Cambridge University Press, Cambridge, 1992)

de Gennes P.G., Prost J., The Physics of Liquid Crystals, (Clarendon Press, Oxford, UK, 1993)

Denniston, C., Orlandini, E. and Yeomans, J. M., (2001). C Simulations of liquid crystals in Poiseuille flow. *Comput. Theor. Polym. Sci.*, Vol. 11 pp. 389-395

de Volder, M., Yoshida, K., Yokota, S., and Reynaerts, D., (2006). J. Micromech. Microeng. Vol. 16, pp. 612.

Doi M. and Edwards S. F., The Theory of Polymer Dynamics (Oxford University Press, New York, 1986)

Ericksen, J. L., : Anisotropic fluids Arch. Ration. Mech. 4,231 (1960)

Frank F. C., (1958). Liquid crystals. On the theory of liquid crystals, Faraday Soc. Discuss. Vil. 25, pp. 19

Forster D., Hydrodynamic Fluctuations, Broken Symmetry and Correlation Functions (Benjamin, Reading, 1975)

Guillén, A.D. & Mendoza, C.I. (2007). Influence of an electric field on the non-Newtonian response of a hybrid-aligned nematic cell under shear flow. The Journal of Chemical Physics, Vol. 126, pp. 204905-1-204905-9; Guillén, A.D. & Mendoza, C.I. (2007). Erratum Influence of an electric field on the non-Newtonian response of a hybrid-aligned nematic cell under shear flow. The Journal of Chemical Physics, Vol. 127, pp. 059901-1-059901-2

Hohenberg P. and Martin P. C., (1965). Microscopic theory of superfluid helium, Ann. Phys. Vol. 34, pp. 291

Kadanoff L. P. and Martin, P. C., (1963). Hydrodynamic equations and correlation functions Ann. Phys. Vol. 24, pp. 419.

Khalatnikov I. M., Introduction to the Theory of Superfluidity (Benjamin, New York, 1965)

Kiss G. and Porter R. S., (1978). Rheology of concentrated solutions of poly(γ-benzyl-glutamate, J. Polym. Sci. Polym. Symp. Vol. 65, pp. 193

Landau L. D. and Lifshitz E., Theory of Elasticity (Pergamon, New York, 1964) 3rd. edition

Leslie F. M., (1966). Some Constitutive equations for anisotropic fluids, Quat.J. Mech. Appl. Math. Vol. 19, pp. 357.

Li, B.; Xu, Y. & Choi, J. (1996). Applying Machine Learning Techniques, *Proceedings of ASME 2010 4th International Conference on Energy Sustainability*, pp. 14-17, ISBN 842-6508-23-3, Phoenix, Arizona, USA, May 17-22, 2010.

Lima, P.; Bonarini, A. & Mataric, M. (2004). *Application of Machine Learning,* InTech, ISBN 978-953-7619-34-3, Vienna, Austria.

Marenduzzo, D., Orlandini, E. and Yeomans, J. M., (2003). Rheology of distorted nematic liquid crystals. *Europhys. Lett*., Vol. 64, pp. 406-412

Marenduzzo, D., Orlandini, E. and Yeomans, J. M., (2004). Interplay between shear flow and elastic deformations in liquid crystals. *J. Chem. Phys*., Vol. 121, pp. 582-591

Marrucci G. and Maffettone P. L., (1989). A description of the liquid-crystalline phase of rodlike polymers at high shear rates, Macromolecules Vol. 22, pp. 4076.

Medina, J.C. & Mendoza, C.I. (2008). Electrorheological effect and non-Newtonian behavior of a homogeneous nematic cell under shear flow: Hysteresis, bistability, and directional response. EPL Europhysics Letters, Vol. 84, pp. 16002-p1-16002-p6

Mendoza, C.I., Corella-Madueño, A., and Reyes, J.A. (2008). Electrorheological effect in a nematic capillary subjected to a pressure gradient, Physical Review E Vol. 77, pp. 011706.

Miesowicz M., (1946). The Three Coefficients of Viscosity of Anisotropic Liquids, Nature Vol. 27, pp. 158.

Negita, K. (1996). Electrorheological effect in the nematic phase of 4-n-pentyl-48-cyanobiphenyl. The Journal of Chemical Physics, Vol. 105, pp. 7837-7841

Parodi O., (1970). Stress tensor for a nematic liquid crystal, J. Phys. (Fr) Vol. 31, pp. 581.

Pleiner H., (1986). Structure of the core of a screw dislocation in smectic A liquid crystals, Liq. Cryst. Vol. 1, pp. 197.

Pleiner H., (1988). Dynamics of a disclination point in smectic-*C* and -*C** liquid-crystal films, Phys. Rev. A Vol. 37, pp. 3986 .

Reyes, J.A.; Manero, O. & Rodriguez, R.F. (2001). Electrorheology of nematic liquid crystals in uniform shear flow. Rheologica Acta, Vol. 40, pp. 426-433

Reyes, J.A., Corella-Madueño, A., and Mendoza, C.I. (2008). "Electrorheological response and orientational bistability for a homogeneously-aligned nematic capillary", The Journal of Chemical Physics Vol. 129, pp. 084710.

Stephen M. J. and Straley J. P., (1974). Physics of liquid crystals, Rev. Mod. Phys. Vol. 46, pp. 617.

Siegwart, R. (2001). Indirect Manipulation of a Sphere on a Flat Disk Using Force Information. *International Journal of Advanced Robotic Systems,* Vol.6, No.4, (December 2009), pp. 12-16, ISSN 1729-8806

Van der Linden, S. (June 2010). Integrating Wind Turbine Generators (WTG's) with Energy Storage, In: *Wind Power,* 17.06.2010, Available from http://sciyo.com/articles/show/title/wind-power-integrating-wind-turbine generators-wtg-s-with-energy-storage

Vicente Alonso, E., Wheeler, A. A. and Sluckin, T. J., (2003). Nonlinear dynamics of a nematic liquid crystal in the presence of a shear flow. *Proc. R. Soc*. London, Ser. A, Vol. 459, pp. 195-220

Zakharov, A.V., Vakulenko, A.A., (2010). Orientational nematodynamics of a hybrid-oriented capillary, Physics of the Solid State Vol. 52, pp. 1542.

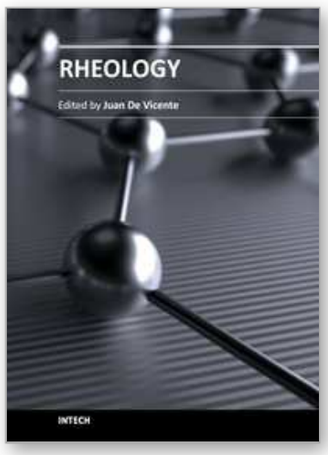

Rheology

Edited by Dr. Juan De Vicente

ISBN 978-953-51-0187-1
Hard cover, 350 pages
Publisher InTech
Published online 07, March, 2012
Published in print edition March, 2012

This book contains a wealth of useful information on current rheology research. By covering a broad variety of rheology-related topics, this e-book is addressed to a wide spectrum of academic and applied researchers and scientists but it could also prove useful to industry specialists. The subject areas include, polymer gels, food rheology, drilling fluids and liquid crystals among others.

InTech Europe
University Campus STeP Ri
Slavka Krautzeka 83/A
51000 Rijeka, Croatia
Phone: +385 (51) 770 447
Fax: +385 (51) 686 166
www.intechopen.com

InTech China
Unit 405, Office Block, Hotel Equatorial Shanghai
No.65, Yan An Road (West), Shanghai, 200040, China
中国上海市延安西路65号上海国际贵都大饭店办公楼405单元
Phone: +86-21-62489820
Fax: +86-21-62489821

IntechOpen